Supplementary Information

Supplementary Methods

Electrophysiology

Coronal brain slices (200-250 μm) were obtained from chicks at P3-7[1]. During experiments, slices were perfused with an artificial cerebrospinal fluid (ACSF, concentrations in mM: 125 NaCl, 2.5 KCl, 26 $NaHCO_3$, 1.25 $NaHPO_4$, 2 $CaCl_2$, 1 $MgCl_2$, and 17 glucose, pH 7.4). Recordings were made using a patch-clamp amplifier (Axopatch 200B, Axon) [1]. Recording temperature was 40 ˚C, the body temperature of birds, for current clamp and 20 ˚C for voltage clamp. Pipettes for whole-cell recordings had a resistance of 3-4 MΩ (3-μm tip diameter) when filled with a KCl-based internal solution (160 KCl, 0.2 EGTA, 10 HEPES-KOH, pH 7.4), while pipettes for cell-attached recordings were 2-3 MΩ (5-μm tip diameter, Fig.1d upper) and contained the ACSF including 4-aminopyridine (2 mM), TEA (3 mM) and Cs^+ (5 mM). Synaptic responses were blocked with 40 μM bicuculline (Sigma) and 40 μM CNQX (Tocris). In voltage-clamp experiments, 4-aminopyridine (0.2 mM), TEA (3 mM) and Cs^+ (5 mM) were included in the bath. Resting potential was assumed to be -60 mV, leak was subtracted, and 3-5 traces were averaged in cell-attached recordings. Antidromic spikes were evoked with a bipolar tungsten electrode placed ventrally to NL. Data were sampled at 20-100 kHz[2].

Immunohistochemistry

Guinea pig anti-chick Nav polyclonal antibodies were raised against synthetic peptides containing a sequence of intracellular III-IV loop for Pan-Nav antibody, and of C-terminus for anti-Nav1.6 antibody. Procedures of immunization and affinity purification were described previously[3]. Mouse monoclonal Pan-Nav antibody (Sigma) and rabbit polyclonal anti-Kv1.2 antibody (Alomone) were commercially obtained. In all cases, immunoreactivity disappeared after pre-adsorption of the antibodies with corresponding peptides. Detailed immunostaining procedures were described previously[4]. NL neurons were retrogradely labeled by stereotaxic injection of Alexa488-conjugated dextran (10,000 MW, Molecular Probes, 10% in PBS) into inferior colliculus of P3-5 chicks under anesthesia (Figs 2d and 2e). Two days after the surgery, sections were prepared for immunohistochemistry.

Computational model

Neuronal modeling and simulation were performed with NEURON 5.6. The model was based on the morphological and electrophysiological data of the chick NL neurons in the high-CF region[4]. Parameters of the model are presented in Supplementary Tables. The model consisted of multiple sections: a soma; 20 dendrites; and an axon with a myelinated initial segment, a hot spot, 10 myelinated internodes, and 10 nodes of Ranvier. K_{LVA} current[5, 6], K_{HVA} current[5, 6],

and Hodgkin-Huxley type Na^+ current[7] followed the web-accessible Model DB[8]. K_{LVA} and K_{HVA} currents were incorporated in soma, dendrites, and unmyelinated segments of axon (hot spot and nodes). Na^+ current was added to the unmyelinated segments of axon. gK_{LVA} and gK_{HVA} in the soma and dendrites were determined according to the observations in high-CF neurons[4]. $V_{1/2}$ of K_{LVA} was set as -50 mV, because 27% of DTX-sensitive conductance was activated at -60 mV[4] (see Supplementary Table 8). $V_{1/2}$ of Na^+ current inactivation (h_{Na}) and gNa, gK_{LVA} and gK_{HVA} in the axon were determined in order to simulate the spike shape and the single spiking nature of high-CF neuron[4], with the arrangement of a hot spot of 10-μm length at a 50-μm distance (Fig.3b, see Supplementary Figs 3 and 4). Density of Na^+ channel in the model was similar to that reported for nodes of Ranvier[9]. Temperature was 40˚C and Q_{10} was 3.0. Time step of calculation was 12.5 μs.

Synaptic conductance has a time profile of an alpha function ($= g_{syn} \cdot t/\tau_{syn} \cdot \exp(1-t/\tau_{syn})$) with a time constant ($\tau_{syn}$) of 0.11 ms, corresponding to that of mEPSCs in high-CF neurons[4] (see Supplementary Table 11). Basic assumptions on synaptic inputs were as follows: NL neurons are multiply innervated and each input is phase-locked to the stimulus sound[10], implying that an NL neuron would receive synaptic inputs of a narrow band width corresponding to its CF. Consistently, field potentials in NL that probably reflect synaptic inputs to a neuron reproduce the tonal stimuli at the corresponding CF region[11]. Timing fluctuation of synaptic inputs was not introduced for simplicity. For binaural stimulation, trains of 50 synaptic inputs were constructed so that the conductance (g_{syn}) was amplitude-modulated between 0.5 and 1 of the maximum value at random with uniform distribution, and two trains with the same patterns were applied into the soma with their phase delay varied. Trains with Gaussian distribution, and with fixed amplitude showed similar results (data not shown). The maximum conductance of synaptic inputs (input conductance) was adjusted to 80-90 nS, so that the maximum firing rate reached 500-600 Hz[12] (see also Fig.3e and Supplementary Fig.8).

Supplementary Tables

Supplementary Table 1 Global parameters

E_{Na}	+50 mV
E_K	-80 mV
E_{leak}	-20 mV
Axial resistance (R_i)	50 Ωcm
Temperature	40 ˚C

Supplementary Table 2 Somatic parameters

Length	20 μm
Diameters	20 μm
Membrane capacitance	2 μF/cm^2
Leak conductance	0.002 S/cm^2
gK_{LVA}	0.006 S/cm^2
gK_{HVA}	0.003 S/cm^2
Number of compartments	1

Supplementary Table 3 Dendritic parameters

Number of dendrites	20
Length	10 μm
Diameters	2 μm
Membrane capacitance	2 μF/cm^2
Leak conductance	0.002 S/cm^2
gK_{LVA}	0.006 S/cm^2
gK_{HVA}	0.003 S/cm^2
Number of compartments	2

Supplementary Table 4 Axon myelinated initial segment parameters

Length	Variable (distance of hot spot; D)
Diameters (proximal)	3 μm
Diameters (distal)	1.3 μm
Membrane capacitance	0.01 μF/cm^2
Leak conductance	10^{-6} S/cm^2
Number of compartments	10

Supplementary Table 5 Axon hot spot parameters

Length	Variable (length of hot spot; L)
Diameters	1.3 μm
Membrane capacitance	1 μF/cm^2
Leak conductance	0.0006 S/cm^2
gNa	16 S/cm^2
gK_{LVA}	0.13 S/cm^2
gK_{HVA}	1.3 S/cm^2
Number of compartments	10

Supplementary Table 6 Axon myelinated internode parameters

Number of internodes	10
Length	80 μm
Diameters	1.3 μm
Membrane capacitance	0.01 μF/cm^2
Leak conductance	10^{-6} S/cm^2
Number of compartments	10

Supplementary Table 7 Axon Ranvier node parameters

Number of nodes	10
Length	2 μm
Diameters	1.3 μm
Membrane capacitance	1 μF/cm^2
Leak conductance	0.0006 S/cm^2
gNa	16 S/cm^2
gK_{LVA}	0.13 S/cm^2
gK_{HVA}	1.3 S/cm^2
Number of compartments	1

Supplementary Table 8 K_{LVA} current parameters (from Neuron Model DB[5, 6, 8])

alpha0	0.2 /ms
alphaVHalf	-50 mV **
alphaK	21.8 mV
beta0	0.17 /ms
betaVHalf	-50 mV **
betaK	14 mV
q10	3 **
T_0	23 ˚C

** indicates parameters modified from the original values (see Supplementary Methods).

Supplementary Table 9 K_{HVA} current parameters

(from Neuron Model DB[5, 6, 8])

alpha0	0.11 /ms
alphaVHalf	-19 mV
alphaK	9.1 mV
beta0	0.103 /ms
betaVHalf	-19 mV
betaK	20 mV
q10	3 **
T_0	23 ˚C

Supplementary Table 10 Na^+ current parameters

(from Neuron Model DB[7-8])

minf	=1 / (1+exp(-(V+38) / 7))
hinf	=1 / (1+exp((V+65) / 6))
mtau	=(10 / (5*exp((V+60) / 18)+36*exp(-(V+60) / 25)))+0.04
htau	=(100 / (7*exp((V+60) / 11)+10*exp(-(V+60) / 25)))+0.6
q10	3
T_0	22 ˚C

Supplementary Table 11 Synaptic input parameters

Number of inputs	50
τ_{syn}*	0.11 ms
Maximum g_{syn}	Variable (indicated in figures)
E_{syn}	+10 mV

* Decay time constant was set as equal to that of mEPSC of high-CF NL neurons; 0.11 ± 0.01 ms (n=12 cells)[4]. This conforms to the value adopted by Grau-Serrat et al. (0.1 ms)[13], and is close to the one reported by Raman et al. in NL (0.12 ms)[14].

Supplementary Figures

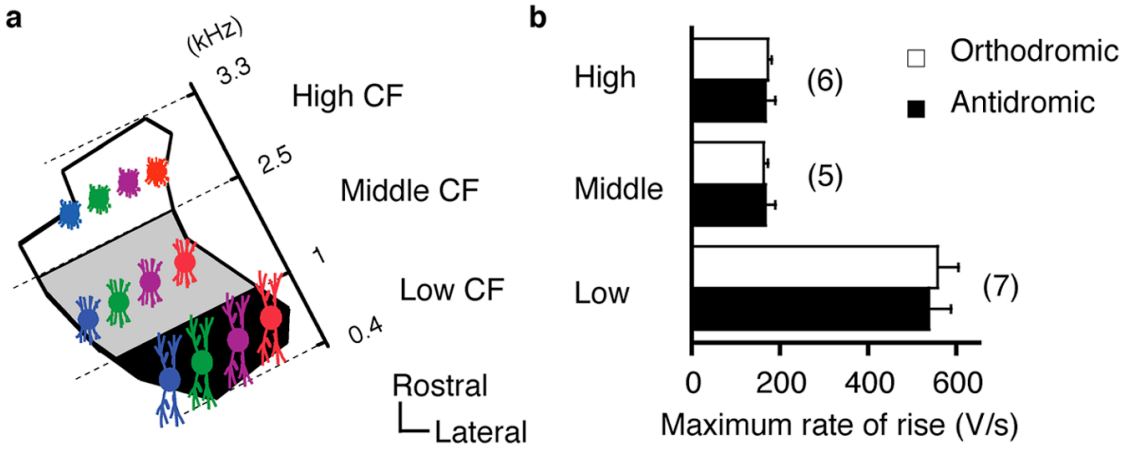

Supplementary Figure 1 Tonotopy in NL and maximum rate of rise of action potentials.

a, Tonotopic arrangement of NL neurons[4, 15]. **b,** There was no difference in the maximum rate of rise between antidromic and orthodromic spikes at each CF.

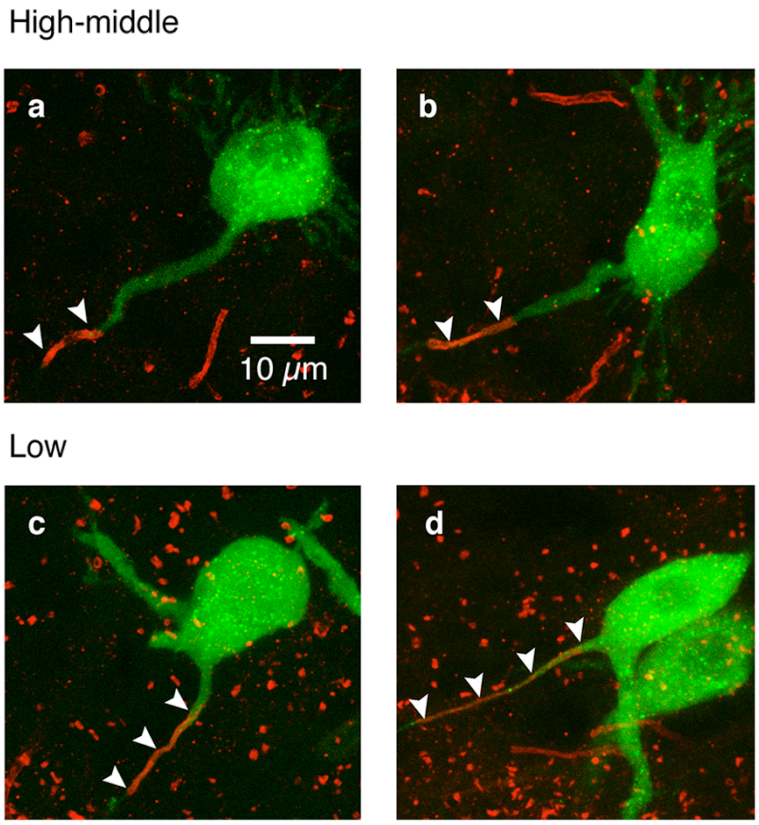

Supplementary Figure 2 Examples of Nav distribution in NL neurons.

Nav channels (red) and retrogradely labeled NL neurons (green). Nav channels are concentrated in the axon (arrowheads) at a more distant site from the soma in high-CF and middle-CF neurons (**a-b**) than in low-CF neurons (**c-d**). NL neurons were retrogradely labelled by Alexa 488-conjugated dextran (10,000 MW) injected into the inferior colliculus.

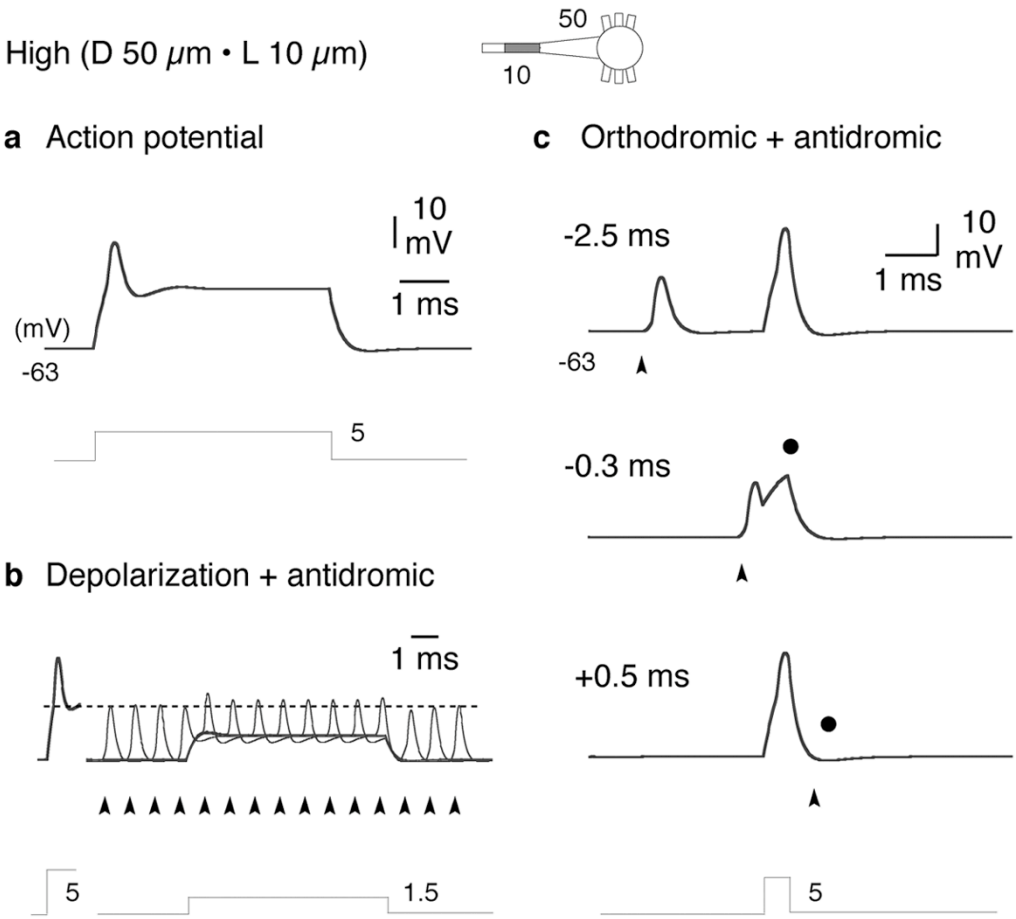

Supplementary Figure 3 Model could reproduce action potentials recorded in high-CF neurons.

a, A somatic current injection of 5-ms duration. No repetitive firings were induced even by the intensified injection (5 nA), as in the experimental observations[4]. Hot spot was of a 10-μm length at a 50-μm distance. **b,** Antidromic spikes during somatic depolarization. **c,** Pairing of antidromic and orthodromic spikes. Arrowheads indicate antidromic spikes. Filled circles indicate failures of spike generation. It should be noted (1) that the site of spike initiation is likely the hot spot rather than the first node of Ranvier; because in simulation, removal of Na^+ current from the hot spot increased the threshold current by more than 50%, while less than 3% by the first node of Ranvier. Also note (2) that effects of the dendritic capacitance on the somatic spike size of high-CF neurons were relatively small; reduction of the dendritic capacitance to 1/10 of the original value increased the somatic spike size by only 25 % (19 mV vs 25 mV).

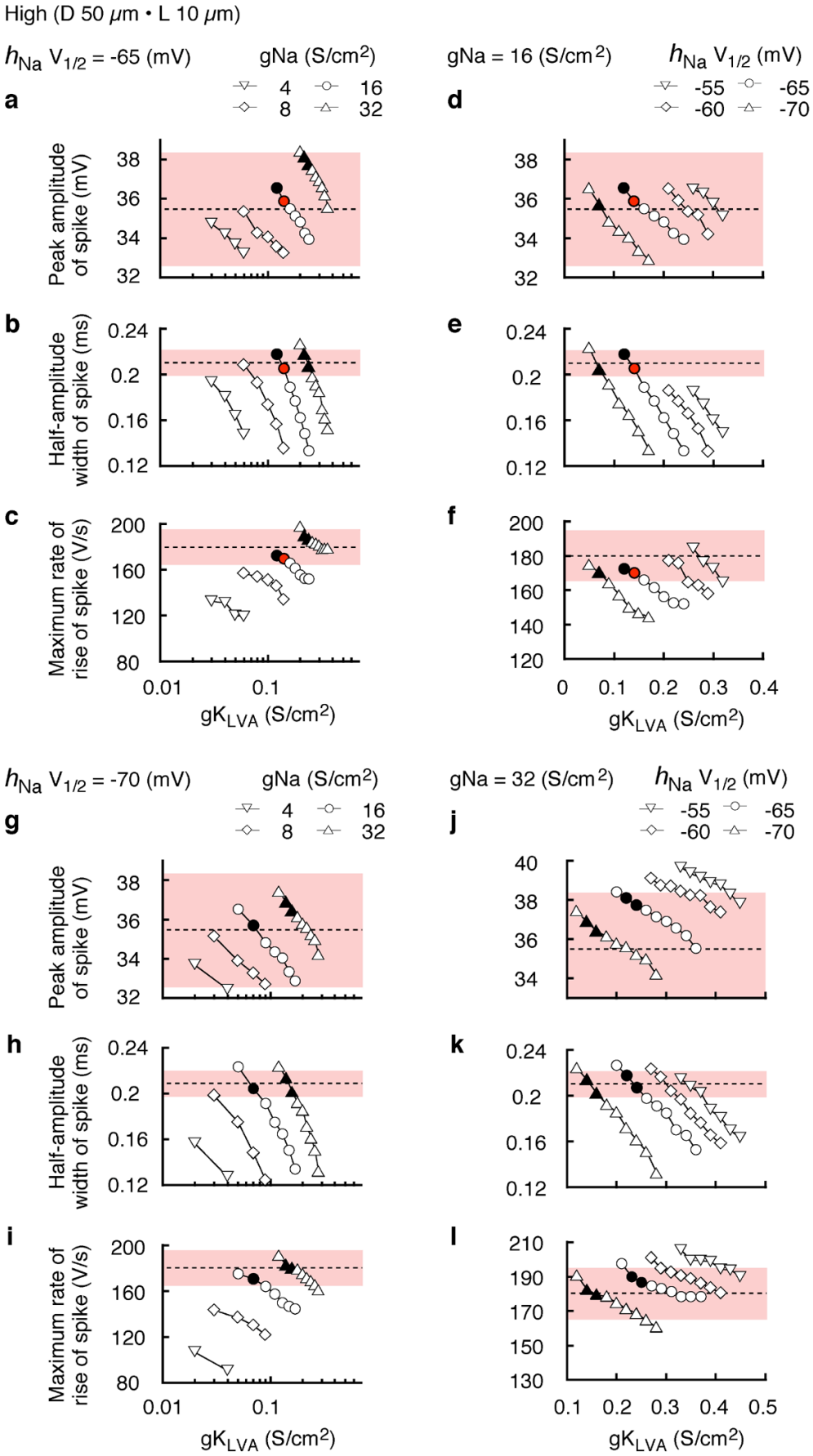
High (D 50 μm • L 10 μm)
h_{Na} $V_{1/2}$ = -65 (mV)
gNa (S/cm²)
4
8
16
32
a
b
c
Peak amplitude of spike (mV)
Half-amplitude width of spike (ms)
Maximum rate of rise of spike (V/s)
gK$_{LVA}$ (S/cm²)
gNa = 16 (S/cm²)
h_{Na} $V_{1/2}$ (mV)
-55
-60
-65
-70
d
e
f
h_{Na} $V_{1/2}$ = -70 (mV)
g
h
i
gNa = 32 (S/cm²)
j
k
l

Supplementary Figure 4 Determination of channel parameters at hot spot.

Three spike parameters (amplitude, half-amplitude width and maximum rate of rise) were calculated as a function of gNa and gK_{LVA} at hot spot (**a-c** and **g-i**), and as a function of $V_{1/2}$ of h_{Na} and gK_{LVA} (**d-f** and **j-l**). A somatic current injection of 5 nA (0.5 ms) was used to elicit spikes. gNa was varied between 4 and 32 S/cm^2, while $V_{1/2}$ of h_{Na} was between -55 and -70 mV. The range of gK_{LVA} variation satisfied the single spiking nature of NL neurons[4] (see Supplementary Methods). Broken lines and red shades indicate means and standard deviations of spike parameters experimentally observed in high-CF neurons (see Text Fig.1 and Supplementary Fig.1b). Red symbols are the parameters adopted in the present model (gNa = 16 S/cm^2, gK_{LVA} = 0.13 S/cm^2, $V_{1/2}$ of h_{Na} = -65 mV). Black symbols indicate other sets of parameters in which all the three spike features are within the observed range (red shades). These indicate that gNa and $V_{1/2}$ of h_{Na} within some restricted ranges (16 or 32 S/cm^2 and -65 or -70 mV, respectively) could reproduce the experimentally observed spikes if gK_{LVA} was appropriately adjusted. We preferred a set of parameters to have the smaller gNa in the present study (16 S/cm^2, red symbols). Note that triangles in **a-c** and **d-f** correspond to circles in **j-l** and **g-i**, respectively. gK_{HVA} was varied in parallel with gK_{LVA} in this and in Supplementary Fig.6 (10 times of gK_{LVA}). The abscissa in **a-c** and **g-i** is the logarithmic scale for visibility.

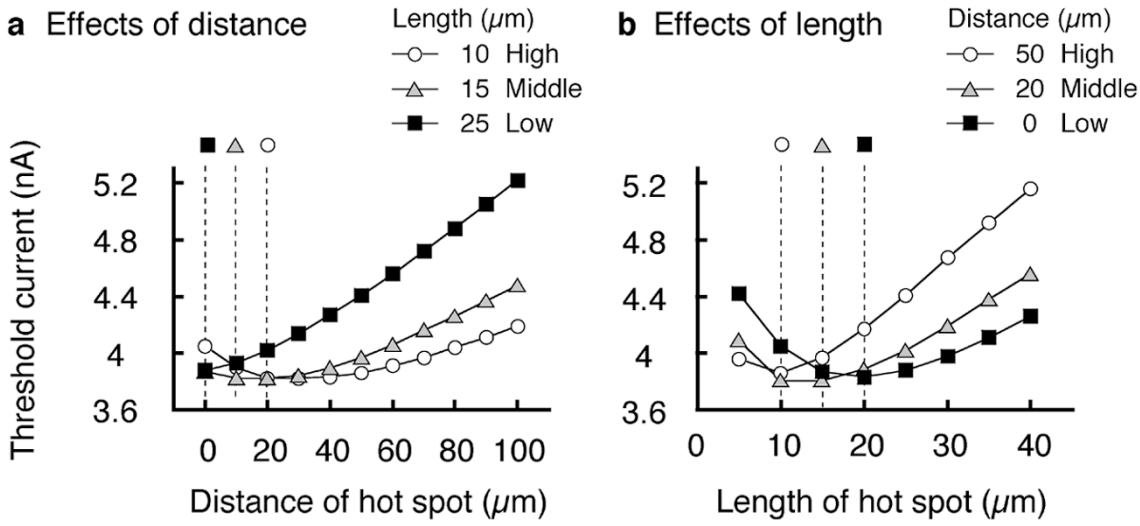

Supplementary Figure 5 Effects of distance and length of hot spot on threshold current.

Threshold current was plotted as a function of distance (**a**) and length (**b**) with the parameters adopted in the present model (Supplementary Fig.4, red). Note that the threshold minimum (broken lines) was given at a more distant location for a short hot spot (10 μm, **a**), and by a shorter length at a distant location (50 μm, **b**). These plots correspond to Text Fig.3c.

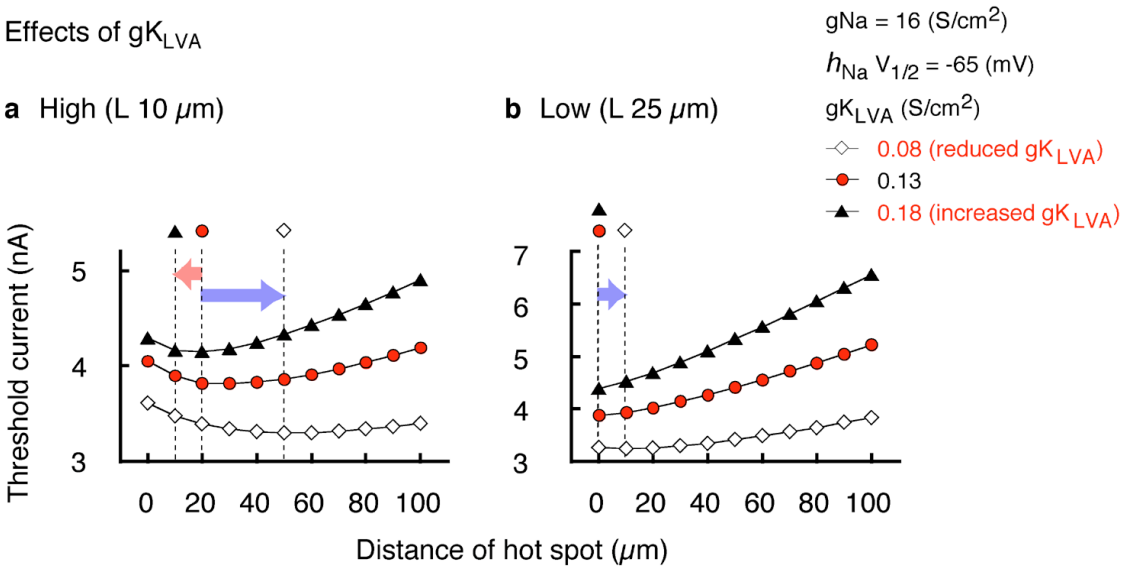

Supplementary Figure 6 Effects of gK$_{LVA}$ at hot spot on threshold current.

Threshold current was calculated as a function of hot spot distance for three different gK$_{LVA}$ values, while gNa and V$_{1/2}$ of h_{Na} were fixed. **a,** High CF (L 10 μm); **b,** low CF (L 25 μm). Note that minimum threshold was more distant in high CF (**a**) than in low CF (**b**) for all the parameters examined. Decrease in gK$_{LVA}$ reduced the threshold current (white diamonds), and the reduction was more robust at a distant hot spot. Consequently, decrease in gK$_{LVA}$ shifted the minimum threshold to a distant location (blue arrows). Increase in gNa or decrease in Na^+ current inactivation reduced the threshold current, but did not affect the threshold-distance profiles critically (data not shown).

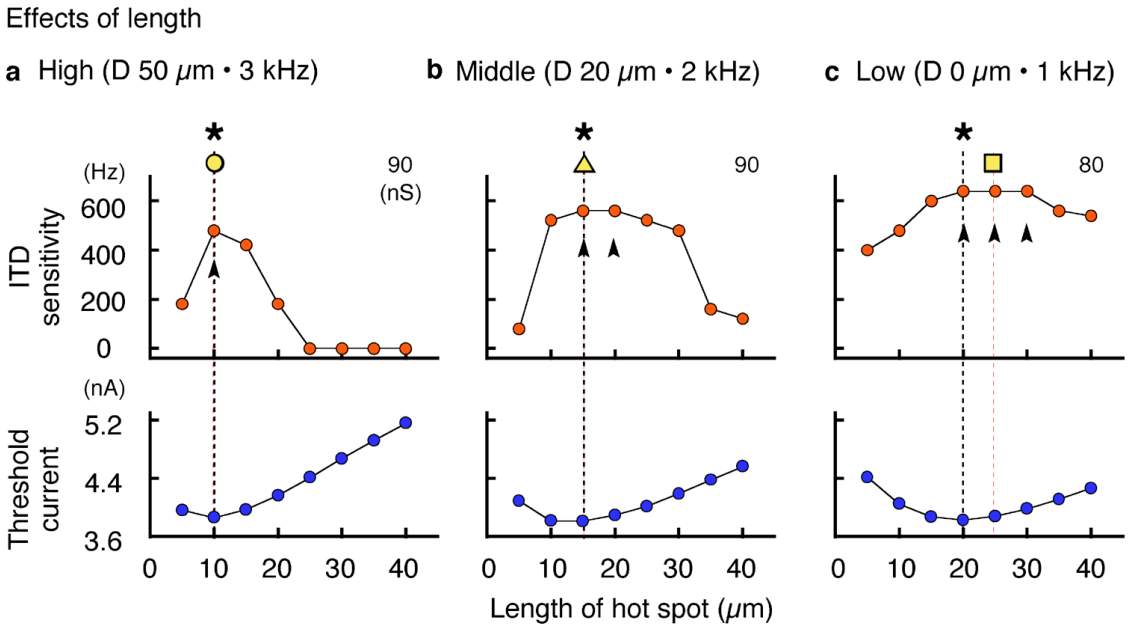

Supplementary Figure 7 Effects of hot spot length on ITD sensitivity.

Hot spot length was varied to see the optimum length in the high-CF (**a**), middle-CF (**b**) and low-CF (**c**) neurons. The distance of the hot spot was fixed to the averages observed at each CF. ITD sensitivity (top) and threshold current (bottom) were plotted as a function of hot spot length. Note that both the maximum ITD sensitivity (arrowheads) and the minimum threshold current (asterisks and black broken lines) matched the length of the observed hot spot (yellow symbols and red broken lines, see Text Fig.2h).

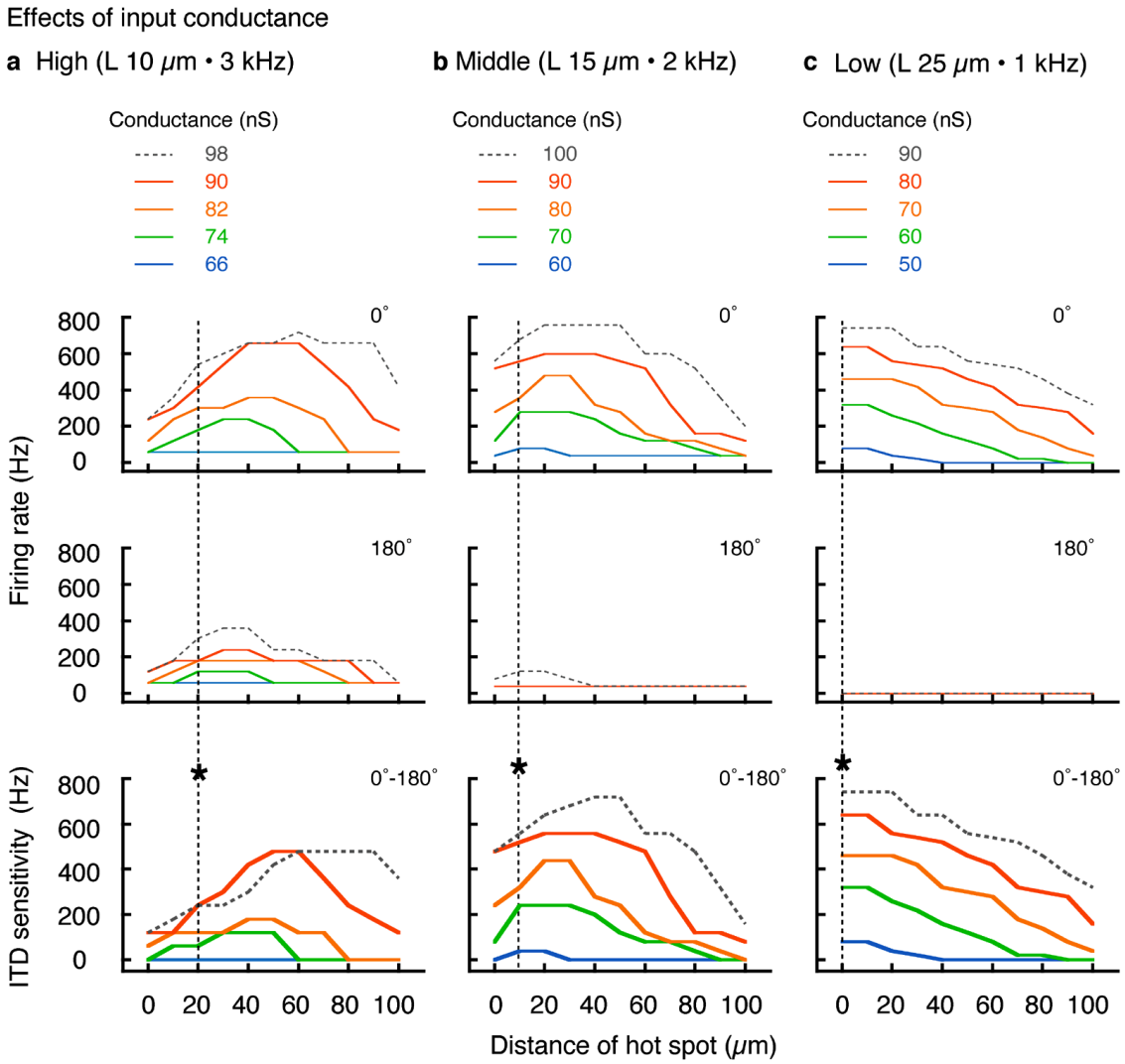

Supplementary Figure 8 Effects of input conductance on ITD sensitivity.

Firing rate of NL neurons was plotted as a function of hot spot distance and input conductance for in-phase (0˚, top) and out-of-phase (180˚, middle) synaptic inputs in high-CF (**a**), middle-CF (**b**) and low-CF (**c**) neurons. Difference of firing rates (0˚-180˚) was defined as ITD sensitivity (bottom). The plots at the bottom extend the range of input conductance presented in Text Figs 3f-h. In the high-CF neurons (**a**), the increase in input conductance increased the firing rate at both in-phase (0˚, top) and out-of-phase stimuli (180˚, middle); the effect was more robust in the in-phase stimulus. Within a stimulus range (66-90 nS, solid lines) to reproduce the firing rate observed in experiments[12] (up to 600 Hz, see Supplementary Methods), the ITD sensitivity (bottom) changed monotonically and the location of its maximum was relatively stable, although a slight distal shift was present (30-50 μm at 74 nS; 50-60 μm at 90 nS). A much stronger stimulus (98 nS, gray dotted lines) displaced the maximum ITD sensitivity to a more distant hot spot (60-90 μm). This was because a strong stimulus increased the firings at both in-phase and out-of-phase, but the effect was more prominent

for the in-phase stimulus when a hot spot was located at a distant site. In the middle-CF neurons (**b**), the firing rate of out-of-phase stimulus was low (180˚) and the distance of the maximum ITD sensitivity was more stable (10-40 μm); a large shift was still observed by an extremely strong stimulus (100 nS, 40-50 μm). In the low-CF neurons (**c**), the maximum ITD sensitivity was found near the soma (0-20 μm) irrespective of the stimulus intensities examined. Asterisks and black vertical broken lines indicate the distance of hot spot to give the minimum threshold current (see Text Figs 3c and f-h).

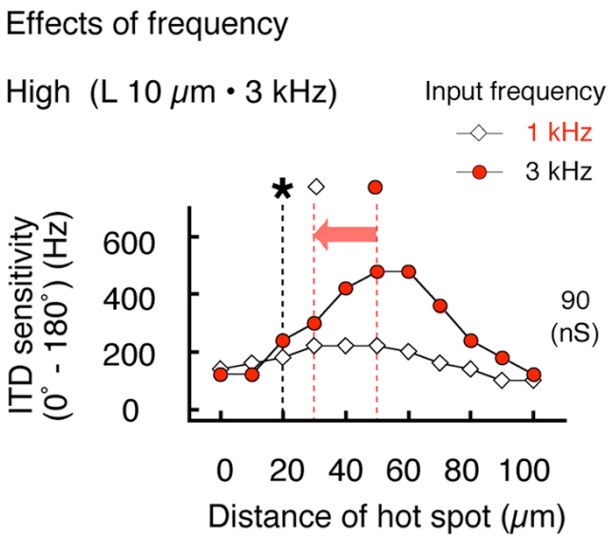

Supplementary Figure 9 Effects of input frequency on ITD sensitivity.

ITD sensitivity was plotted as a function of hot spot distance in high-CF neurons. Red symbols correspond to Text Fig.3f. Phase delay at 180˚ was set as 0.17 ms, corresponding to CF of 3 kHz, irrespective of the input frequency. Sparse inputs (1 kHz, 90 nS) reduced the extent of plateau depolarization at the soma (11 mV, white diamonds) and shifted the location of maximum ITD sensitivity to a closer site (30-50 μm) compared with 3-kHz inputs (22 mV, 50-60 μm, red circles). However, the location was still more distant than the threshold minimum (20 μm, asterisk). Sparse inputs reduced the ITD sensitivity, because the firing rates were not largely different between in-phase (0˚) and out-of-phase (180˚). Decrease in the input frequency and the conductance of synaptic inputs (Supplementary Fig.8) might be equivalent to the decreased intensity of sound stimulus.

References for Supplementary Information

1. Kuba, H., Koyano, K. & Ohmori, H. Development of membrane conductance improves coincidence detection in the nucleus laminaris of the chicken. *J. Physiol. (Lond.)* **540,** 529-542 (2002).

2. Kuba, H., Yamada, R. & Ohmori, H. Evaluation of the limiting acuity of coincidence detection in nucleus laminaris of the chicken. *J. Physiol. (Lond.)* **552,** 611-620 (2003).

3. Yamada, R., Kuba, H., Ishii, T. M. & Ohmori, H. Hyperpolarization-activated cyclic nucleotide-gated cation channels regulate auditory coincidence detection in nucleus laminaris of the chick. *J. Neurosci.* **25,** 8867-8877 (2005).

4. Kuba, H., Yamada, R., Fukui, I. & Ohmori, H. Tonotopic specialization of auditory coincidence detection in nucleus laminaris of the chick. *J. Neurosci.* **25,** 1924-1934 (2005).

5. Rathouz, M. & Trussell, L. Characterization of outward currents in neurons of the avian nucleus magnocellularis. *J. Neurophysiol.* **80,** 2824-2835 (1998).

6. Simon, J. Z., Carr, C. E. & Shamma S. A. A dendritic model of coincidence detection. *Neurocomputing* **26-27,** 263-269 (1999).

7. Rothman, J. S. & Manis, P. B. The roles potassium currents play in regulating the electrical activity of ventral cochlear nucleus neurons. *J. Neurophysiol.* **89,** 3097-3113 (2003).

8. Hines, M. L., Morse, T., Migliore, M., Carnevale, N. T. & Shepherd, G. M. Model DB: a database to support computational neuroscience. *J. Comput. Neurosci.* **17,** 7-11 (2004).

9. Vogel, W. & Schwartz, J. R. in *The Axon* (eds Waxman, S. G., Kocsis, J. D. & Stys, P. K.) 257-280 (Oxford University Press, Oxford, NY, 1995).

10. Warchol, M. E. & Dallos, P. Neural coding in the chick cochlear nucleus. *J. Comp. Physiol. A* **166,** 721-734 (1990).

11. Schwarz, D. W. F. Can central neurons reproduce sound waveforms? An analysis of the neurophonic potential in the laminar nucleus of the chicken. *J. Otolaryngol.* **21,** 30-38 (1992).

12. Pena, J. L., Viete, S., Albeck, Y. & Konishi, M. Tolerance to sound intensity of binaural coincidence detection in the nucleus laminaris of the owl. *J. Neurosci.* **16,** 7046-7054 (1996).

13. Grau-Serrat, V., Carr, C. E. & Simon, J. Z. Modeling coincidence detection in nucleus laminaris. *Biol. Cybern.* **89,** 388-396 (2003).

14. Raman, I. M., Zhang, S. & Trussell, L. O. Pathway-specific variants of AMPA receptors and their contribution to neuronal signalling *J. Neurosci.* **14,** 4998-5010 (1994).

15. Rubel, E. W. & Parks, T. N. Organization and development of the brain stem auditory nuclei of the chicken: tonotopic organization of N. magnocellualris and N. laminaris. *J. Comp. Neurol.* **164,** 411-434 (1975).